Synthesis and Characterisation of Hydrated Calcium Pyrophosphate Phases of Biological Interest

Pierre Gras, Christian Rey, Olivier Marsan, Stéphanie Sarda, Christèle Combes

DOI:10.1002/ejic.201300955

Synthesis and Characterisation of Hydrated Calcium Pyrophosphate Phases of Biological Interest

Pierre Gras,[a] Christian Rey,[a] Olivier Marsan,[a] Stéphanie Sarda,[b] and Christèle Combes*[a]

Keywords: Biological calcification / Physicochemical characterization / Calcium pyrophosphate / Synthetic methods / Hydrates / Vibrational spectroscopy

The details of a synthesis method for biologically relevant hydrated calcium pyrophosphates (CPPs, $Ca_2P_2O_7{\cdot}nH_2O$) has been elucidated. Control of the pH (from 3.6 to 5.8) and the temperature (from 25 to 90 °C) during the synthesis enabled the preparation of four pure CPP phases within one hour without intermediates: monoclinic and triclinic calcium pyrophosphate dihydrate (CPPD, $Ca_2P_2O_7{\cdot}2H_2O$), which are the two CPP phases detected in vivo in joints of arthritic patients, monoclinic tetrahydrate β (CPPT, $Ca_2P_2O_7{\cdot}4H_2O$) and an amorphous phase (a-CPP, $Ca_2P_2O_7{\cdot}nH_2O$). Four domains corresponding to the four different phases of hydrated calcium pyrophosphate were identified; a-CPP was synthesised over a very wide pH and temperature range (up to 90 °C) within the domain of synthesis conditions explored, including physiological conditions (pH 7.4 and 37 °C). The as-synthesised hydrated CPP phases were characterised by complementary techniques (powder X-ray diffraction, FTIR and Raman spectroscopy, scanning electron microscopy and thermogravimetry) and chemical analyses. Rietveld refinement analyses of the as-synthesised crystalline phases were performed, and there were significant differences between the m-CPPD X-ray diffraction pattern observed and previously published cell parameters. Vibrational spectroscopy allowed the crystalline and amorphous phases synthesised to be clearly distinguished and identified owing to the high flexibility of the pyrophosphate anion. Chemical analyses showed that the synthesis conditions used in this study did not allow significant hydrolysis of the pyrophosphate ions into phosphate ions, and the number of water molecules associated with each synthesised CPP phase was determined by thermogravimetric analysis. Different mechanisms of dehydration were also identified. The study of the formation of synthetic and well-characterised hydrated calcium pyrophosphate phases and their availability in large amounts in vitro could allow progress to be made on the biological role of these phases and their possible transformations. This could also aid their detection in patients suffering from disease caused by calcium salt crystals and could clarify the mechanism by which CPP crystals form and evolve in vivo.

Introduction

Calcium pyrophosphate hydrates (CPP, $Ca_2P_2O_7{\cdot}nH_2O$) are involved in several forms of arthritis, including calcium pyrophosphate crystal deposition disease, also known as pseudogout, and osteoarthritis (OA), the most frequent form of rheumatic disease.[1,2] To date, two different polymorphs of dihydrate CPP crystals are commonly identified in joint tissues of arthritic patients: monoclinic and triclinic calcium pyrophosphate dihydrate (CPPD, $Ca_2P_2O_7{\cdot}2H_2O$) crystals, referred to as m-CPPD and t-CPPD, respectively. They have been reported in a large range of sizes, typically from 0.06 to 0.3 μm in the temporomandibular joint and from ca. 1 to 20 μm in the knee.[3,4] They both appear to induce an inflammatory response, possibly because of the rupture of lysosome phospholipid membranes induced by pyrophosphate groups on the surface of the crystals.[5–8] However, current treatments cannot inhibit the formation of CPP crystals, although they help to resolve the inflammatory responses.[9–11]

Although many papers have focused on CPP crystals associated with OA from a clinical point of view, very little in the way of physicochemical data on these phases of biological interest has been published. Several in vitro syntheses of hydrated CPP have been reported.[12–20] They were mainly based on the method developed by Brown et al.[12] and its modifications by Mandel et al.[13] Four calcium pyrophosphate hydrates were reported among the 25 calcium-containing pyrophosphate compounds described in the literature,[12] including m-CPPD, t-CPPD, a dimorphic monoclinic tetrahydrate (CPPT, $Ca_2P_2O_7{\cdot}4H_2O$) referred to as m-CPPT α and m-CPPT β.[21,22]

However, these methods present some drawbacks as they lead to low total reaction yields and generally involve unstable calcium pyrophosphate intermediates, as highlighted by Groves et al.[20] Other methods were developed to overcome either or both of these disadvantages, especially for

[a] CIRIMAT, INPT-CNRS-UPS, Université de Toulouse, ENSIACET,
31030 Toulouse, France
E-mail: christele.combes@ensiacet.fr
[b] CIRIMAT, INPT-CNRS-UPS, Université Paul Sabatier,
31062 Toulouse, France

the synthesis of t-CPPD, m-CPPT β and an amorphous phase (a-CPP), but not for m-CPPD.[20,23,24] However, the crystalline phases are obtained with synthesis durations between two hours and one week, and the reproducibility of some of these methods is rather unpredictable and the pure phases are not always obtained.[25,26] There is an interest in studying the conditions of formation of all these hydrated CPP phases in vitro and in finely characterising them to better understand their formation in vivo (direct formation or possibly the hydrolysis and evolution of a metastable precursor phase). We recently reported the synthesis of m-CPPT β at pH 4.6 and 25 °C by a fast and simple synthesis method.[27] On the basis of this synthesis method, we could suggest that a variation of pH and temperature leads to the formation of pure pathological CPP phases, that is m-CPPD and t-CPPD.

In the present study, we investigated the formation conditions of hydrated calcium pyrophosphate phases obtained by a single-step precipitation in aqueous media. The four different forms obtained, m-CPPD, t-CPPD, m-CPPT β and a-CPP, were characterised by physicochemical methods and techniques including powder X-ray diffraction (XRD), FTIR and Raman spectroscopy, thermogravimetric and differential thermal analyses (TGA-DTA), scanning electron microscopy (SEM), the Brunauer–Emmett–Teller (BET) method for specific surface area determination and chemical analyses (calcium and phosphate titration).

Results and Discussion

Synthesis

The synthesis method implemented in the present study could be described as a direct (without intermediates) synthesis method for several hydrated calcium pyrophosphate phases. The double decomposition of the calcium nitrate and potassium pyrophosphate solutions occurs in an aqueous buffered medium containing ammonium and acetate ions. The precipitation reaction involved can be represented by Equation (1).

$$2Ca^{2+} + P_2O_7^{4-} \rightarrow Ca_2P_2O_7{\cdot}nH_2O \quad (1)$$

Generally, the two most important parameters involved in the precipitation of various salts in different hydration states are temperature and pH. Our study focuses on the influence of these parameters, which were not systematically explored and described in previous works related to CPP synthesis. Although other parameters, such as stirring or reagent concentration, may determine the nature of the phases formed, most of our syntheses were performed with a stoichiometric calcium/pyrophosphate ratio of 2 and with magnetic stirring. Briefly, we investigated the influence of the method of addition of reagents into the buffer, especially the influence of concentration of the reagent solutions.

The influence of pH and temperature was studied by performing several experiments with pH varied from 3.6 to 5.8 and temperature varied from 25 to 90 °C at fixed concentrations. Samples from these experiments were analysed by FTIR spectroscopy and powder XRD (data not shown) and compared with data already published.[12,13,22,24,28]

Figure 1 shows the formation domains of pure hydrated CPP phases for our synthesis method. At fixed concentrations of pyrophosphate and calcium (75 and 150 mmol L^{-1}, respectively, in reagent solution), we determined four domains corresponding to four different phases of hydrated calcium pyrophosphate: a-CPP, an amorphous phase, m-CPPT β, a tetrahydrated phase, both formed at low temperatures, and m-CPPD and t-CPPD, two biologically relevant phases synthesised at higher temperatures (Figure 1). Mixtures of these phases (generally two CPP phases, including a-CPP and poorly crystalline phases for pH above 4.5 and temperature under 70 °C) were obtained under pH and temperature conditions corresponding to the areas between the domains of pure CPP formation.

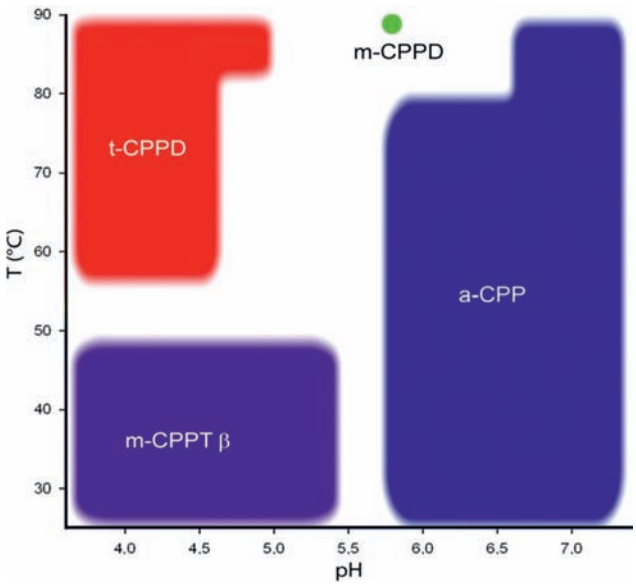

Figure 1. Synthesis domains of the four pure hydrated CPP phases. Mixtures of these phases were obtained under conditions outside these domains.

The CPP crystalline compounds synthesised under these conditions have coherent domains over 50 nm in at least one direction, as determined by using the Scherrer equation. No morphological differences have been observed with modification of temperature for each formation domain, but synthesis under more acidic conditions promotes growth of well-faceted plates for m-CPPT β and thicker and longer needles for t-CPPD.

Several syntheses of pyrophosphate hydrates with the general formula $M_2P_2O_7{\cdot}nH_2O$, in which M is a bivalent metal, have been reported: these include condensation of hydrogen phosphate ions HPO_4^{2-},[29–32] precipitation processes, the use of ion-exchange resins[33,34] and double decomposition. In these cases, the product was then allowed to stand for several hours to crystallise into the desired

phase. Double decomposition has been used to form amorphous and then crystalline pyrophosphate compounds of manganese pyrophosphate, $Mn_2P_2O_7{\cdot}nH_2O$,[35] amorphous cobalt pyrophosphate, $Co_2P_2O_7{\cdot}nH_2O$, which was used as an intermediate for the synthesis of crystalline compounds such as $Co_2P_2O_7{\cdot}6H_2O$,[36] and calcium pyrophosphate (CPP), which was formed as an amorphous hydrated phase a-CPP and then crystallised into two dimorphs of $Ca_2P_2O_7{\cdot}2H_2O$ (t-CPPD and m-CPPD) and two dimorphs of $Ca_2P_2O_7{\cdot}4H_2O$ (m-CPPT α and m-CPPT β).[12,20,23,24]

The coprecipitation of calcium and pyrophosphate ions at room temperature and without monitored pH leads to an amorphous phase.[12,20,24] We showed that the amorphous phase can also be synthesised by our method within a wide range of temperatures and pH (from ambient temperature to 90 °C and from pH 5.8 to 7.4) with no evidence of crystallisation (Figure 1).

Interestingly, this amorphous calcium salt can precipitate at much higher temperature than amorphous calcium orthophosphate or amorphous calcium carbonate, which are also amorphous calcium salts of biological interest. Unlike these latter amorphous phases, which may crystallise readily even at room temperature, a-CPP did not crystallise during the 45 min of synthesis at 90 °C or if kept in the mother liquor for over 6 months at room temperature. This stability could be explained by the flexible structure and probably the size of the $P_2O_7^{4-}$ anion, which could enhance inhibition of crystallisation of a-CPP compared to the CO_3^{2-} or PO_4^{3-} anions in calcium carbonate and calcium phosphate salts, respectively.[24] The highly flexible P–O–P bond has been reported with angles varying from 123° to 180° in the solid state.[37]

However, it has been reported that the amorphous phase then crystallised within one day to one week under specific conditions into the different crystalline forms already mentioned.[12,13,20] Thereby, the published synthesis methods of crystalline CPP are mostly based on the dissolution of an intermediate, amorphous CPP (a-CPP) or calcium dihydrogen pyrophosphate ($CaH_2P_2O_7$), followed by crystallisation into the CPP phase by using different synthesis conditions (pH temperature, concentration, agitation, time). These syntheses were performed for more than 24 h and led to low total reaction yields.[20]

The method we set up for the m-CPPT β and t-CPPD syntheses used conditions already described to lead to this phase from a-CPP as intermediate: temperature below 50 °C and pH above 5 for m-CPPT β, and in acidic medium and the use of a steam bath for t-CPPD.[12,13,20,23] However, the synthesis described in this study was achieved in one step within 45 min, as with the other three phases synthesised, and was faster than the 24 h to one week needed for the previously published methods.

The synthesis method also allowed synthesis of the m-CPPD phase, a biologically relevant phase that has been observed in several joints of arthritic patients in addition to t-CPPD[4] and appears to have greater inflammatory properties than t-CPPD.[5,6] m-CPPD has been poorly studied in the literature; the synthesis methods already published often involve Mg^{2+} ions or lead to a mixture of m-CPPD and t-CPPD phases.[12–15,25]

Figure 1 shows that the conditions for m-CPPD synthesis were very narrow: lower pH values and temperatures during the synthesis lead to the formation of m-CPPT β instead of the dihydrate and higher pH values and temperatures lead to t-CPPD, as already mentioned.[12] The synthesis conditions of pH 5.8 and 90 °C allowed the formation of the m-CPPD phase, and the reaction time was fast enough to avoid the transition into t-CPPD mentioned by Brown et al.[12] In water, m-CPPD and m-CPPT β were reported to slowly evolve to the t-CPPD phase. However, we determined that if m-CPPD was kept in the mother liquor at 50 °C for over 1 month, the as-synthesised m-CPPD phase does not evolve into t-CPPD.

Interestingly, the synthesis of m-CPPD described in the present study occurred without the addition of Mg^{2+} ions to the solution; however, the nature of the crystals formed was reported to be highly dependent on the concentration of Mg^{2+} ions, which are the main impurity in commercial calcium salts. The calcium nitrate salt we used contained less than 100 ppm Mg^{2+} ions (manufacturer analysis). High concentrations of magnesium ions are known to favour m-CPPD formation, as reported by Cheng et al.,[15,38] and magnesium ions are used for this purpose in the method developed by Mandel et al.[13] However, pyrophosphate ions are approximately five times more effective in sequestering magnesium ions than calcium ions and could lead to impurities in the crystals.[39] This point could partially explain why it is difficult to obtain a pure m-CPPD phase and why the structure of this phase is still unresolved 50 years after its first preparation and XRD characterisation.[4] Thus, we briefly investigated the influence of different parameters on the synthesis of m-CPPD.

Different molar ratios of calcium/pyrophosphate (from $[Ca^{2+}] = [P_2O_7^{4-}]$ to $[Ca^{2+}] = 4[P_2O_7^{4-}]$ with $[Ca^{2+}] = 150\ mmol\,L^{-1}$) were used at fixed pH and temperature corresponding to the conditions for the formation of m-CPPD (pH 5.8 and 90 °C).

A mixture of m-CPPD and t-CPPD appeared at $[Ca^{2+}] = 1.5[P_2O_7^{4-}]$ and below, and an amorphous phase formed for $[Ca^{2+}] = 3[P_2O_7^{4-}]$ and above.

It should also be noted that if the calcium solution was added to the buffered pyrophosphate reagent with $[P_2O_7^{4-}] = 75\ mmol\,L^{-1}$, that is, with a large excess of pyrophosphate ions compared to calcium ions, a phase identified as a pentacalcium diammonium pyrophosphate hexahydrate, $Ca_5(NH_4)_2(P_2O_7)_3{\cdot}6H_2O$, formed.

Physicochemical Characterisation of as-Synthesised Pure CCP Phases

Four samples, one for each pure CPP phase synthesised at pH and temperature within their respective domain of formation, were selected for further characterisation. These samples correspond to the synthesis conditions reported in Table 1.

Table 1. Synthesis temperature and pH of the selected samples further characterised by powder XRD and FTIR spectroscopy ([Ca^{2+}] = 2[$P_2O_7^{4-}$] = 150 mM).

	a-CPP	m-CPPD β	m-CPPD	t-CPPD
Temperature [°C]	25	25	90	90
pH	5.8	4.5	5.8	3.6

The crystalline samples selected were identified by powder X-ray diffraction analysis (Figure 2) as m-CPPT β, m-CPPD and t-CPPD by the characteristic pattern of each phase according to the published data (Table 2).[13,22,28] A fourth pattern, including a broad diffuse halo was also observed and is characteristic of an amorphous phase (a-CPP).

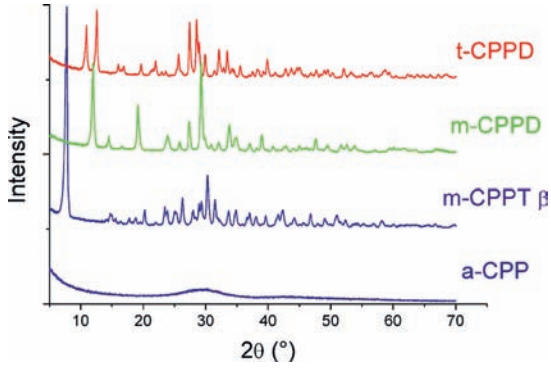

Figure 2. XRD patterns of the hydrated calcium pyrophosphate phases synthesised.

The pattern obtained for the m-CPPD phase was in good agreement with the data published by Brown et al. and the patterns published by Liu et al.[12,19] but did not correspond to the lattice constant determined by Mandel et al.[13] The structure of m-CPPD has not been resolved, even though m-CPPD has been identified in arthritic joints.[5,25]

Rietveld refinements were performed on the X-ray diffraction patterns of the as-synthesised m-CPPD and were based on the dihydrate pyrophosphate compound cell parameters from other monoclinic pyrophosphate dihydrate structures fully identified as $Mg_2P_2O_7{\cdot}2H_2O$,[30] $Co_2P_2O_7{\cdot}2H_2O$,[31] $Fe_2P_2O_7{\cdot}2H_2O$[32] and $Mn_2P_2O_7{\cdot}2H_2O$,[35] which share very similar cell parameters and atomic organisation.

However, no satisfactory cell parameters similar to those of the $X_2P_2O_7{\cdot}2H_2O$ structures were found from the powder X-ray diffraction pattern; therefore, the m-CPPD structure could be significantly different from those of the other dihydrate pyrophosphate compounds (Table 2).

FTIR and Raman spectroscopy allow clear identification of pyrophosphate compounds and provide valuable information on the confirmation of the pyrophosphate ion. Thus, thanks to the flexibility of the pyrophosphate anion in the structure, these methods provide an effective means to clearly identify calcium pyrophosphate hydrates. Figures 3 and 4 show FTIR and Raman spectra, respectively, of the four as-synthesised hydrated CPP phases; the positions and assignments of the IR and Raman bands for the three crystalline hydrated CPP phases are reported in Table 3.

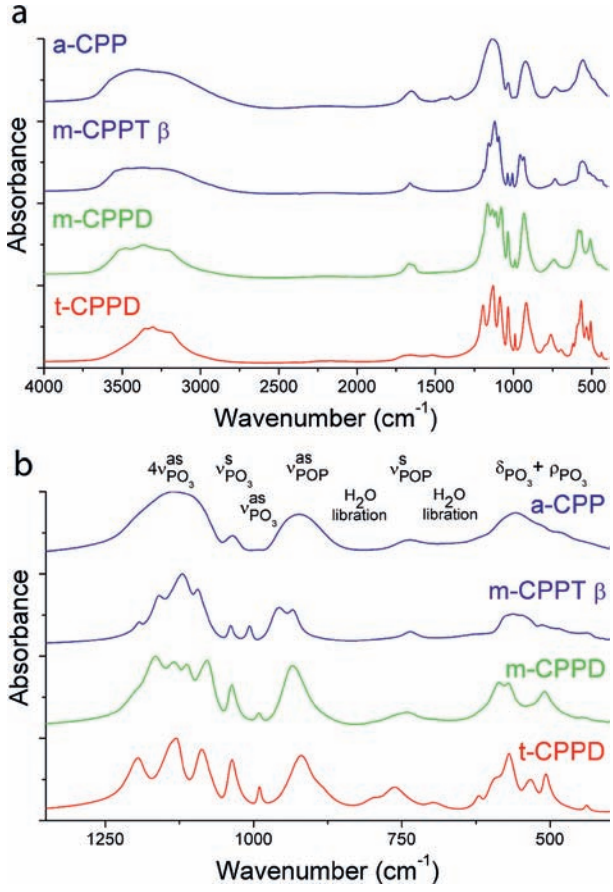

Figure 3. FTIR spectra of the four hydrated calcium pyrophosphate phases synthesised. (a) 4000–400 cm^{-1} domain, (b) 1300–500 cm^{-1} domain.

Although Cornilsen predicted 21 Raman and 21 IR active modes of $P_2O_7^{4-}$ for t-CPPD,[40] these vibrations could not be separated in the spectra, and the data are discussed with regard to the vibrational domains of the free

Table 2. Unit-cell parameters obtained by Rietveld refinement for the m-CPPT β, t-CPPD and m-CPPD samples compared to the single crystal data from Balić-Žunić et al. and Mandel.[22,28] Estimated standard deviations are given in parentheses.

	Ref.	R_p/R_{wp}	a [Å]	b [Å]	c [Å]	α [°]	β [°]	γ [°]
m-CPPT β	refined	0.0614/0.0789	12.288(1)	7.512(1)	10.776(1)	90.00	112.51(1)	90.00
	[22]		12.287(6)	7.511(3)	10.775(5)	90.00	112.54(1)	90.00
t-CPPD	refined	0.0538/0.0684	7.359(5)	8.279(6)	6.690(5)	102.87(1)	72.73(1)	94.96(1)
	[28]		7.365(4)	8.287(4)	6.691(4)	102.96(1)	72.73(1)	95.01(1)
m-CPPD	refined	0.0772/0.1020	12.618(1)	9.250(1)	6.760(1)	90.00	104.97(1)	90.00

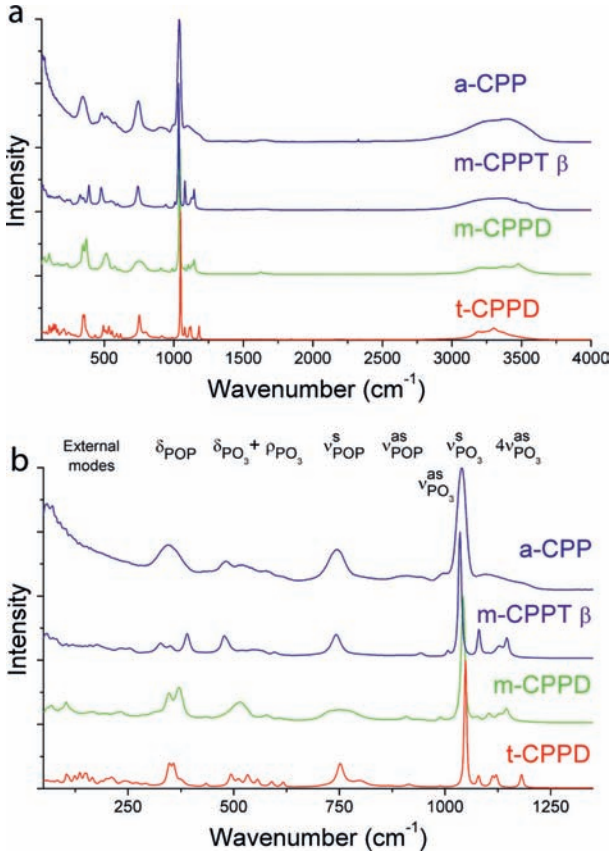

Figure 4. Raman spectra of the four hydrated calcium pyrophosphate phases synthesised. (a) 400–4000 cm^{-1} domain, (b) 500–1300 cm^{-1} domain.

Table 3. Vibrational band position [cm^{-1}] assignments and calculated P–O bond lengths for m-CPPD, t-CPPD and m-CPPT β.

t-CPPD		m-CPPT β		m-CPPD		Assignment
IR	Raman	IR	Raman	IR	Raman	
3576	3578	3615		3521	3525	
3511	3511	3551	3547	3476	3476	
3471	3464	3488		3366	3368	
3361	3368	3364	3386	3309		ν_{OH}
3305	3300	3263	3242	3249	3251	
3244	3242	3178	3168	3188	3193	
3182	3182	3047	3050			
1711		1662	1664	1669	1665	
1660		1620		1636	1628	δ_{HOH}
1522						
1195	1182	1193		1206		
1140	1121	1159	1147	1165	1147	
1130	1113	1120	1128	1134	1131	ν^{as}_{PO3}
1088	1080	1094	1101	1121	1106	
			1079	1078	1076	
1037	1049	1035	1036	1036	1045	ν^{s}_{PO3}
990	990	1007	1008	991	992	ν^{as}_{PO3}
920	916	957	945	934	941	
880	890	934				ν^{as}_{POP}
798	797			802		H_2O libration
762	753	736	743	767	775	
				739	725	ν^{s}_{POP}
696	705			691		H_2O libration
621	618	621	597	625	611	
594	590	576	573	589	579	
569	557	561	562	569	571	
534	533	549	547	509	518	$\delta_{PO3} + \rho_{PO3}$
507	512	513	518	442	433	
493	493	488	479			
438	436	440				

ion. Eight P–O stretching modes can be distinguished in the following order of frequencies and assignments: four $\nu^{as}PO_4 > \nu^{s}PO_4 > \nu^{as}PO_4 > \nu^{as}POP > \nu^{s}POP$ (Figures 3, a and 4). P–O and P–O–P stretching vibration bands were observed between 1250 and 950 cm^{-1} and between 950 and 700 cm^{-1}, respectively, in the spectra of t-CPPD, m-CPPT β and m-CPPD (Table 3).

These $P_2O_7^{4-}$ vibration modes were observed for all three crystalline samples (t-CPPD, m-CPPT β and m-CPPD) by IR and/or Raman spectroscopy. The band positions are somewhat distinct and allowed unambiguous attribution of the bands for each hydrated CPP phase.

As already noted, the 21 predicted active modes are not all apparent, although several bands present shoulders. In particular, the $\nu^{as}POP$ vibration in the FTIR spectra seems to be coupled with another band, and this is especially apparent for m-CPPT β. This band was not observed in the Raman spectra.

Water O–H vibrations occurred in the 3700–2800 cm^{-1} region, and there are significant differences between the spectra of the synthesised pure CPP phases. This region of the m-CPPD spectrum seemed closer to the spectrum of m-CPPT β, a tetrahydrate with layers composed of water molecules, than to that of t-CPPD, another dihydrate. A weak broad adsorption band also appeared in the 2400–1950 cm^{-1} range. In the absence of H_3O^+ ions and P–O–H groups in the crystal, this band was presumed to correspond to composite vibration of water molecules $(\delta + \omega)_{OH}$.[41]

The spectroscopic data also allow direct information about the $P_2O_7^{4-}$ configuration to be obtained, and especially the P–O–P bond angle, as proposed by Rulmont et al.[37] In t-CPPD and m-CPPT β, the $P_2O_7^{4-}$ anions have a bent P–O–P angle and an eclipsed configuration. In particular, the P–O–P angle has been reported as 123.1° for t-CPPD and 134.1° for m-CPPT β, both in the dichromate configuration.[22,28] The $P_2O_7^{4-}$ anion could be considered as a three-body system, mainly by disregarding couplings between the vibrations of the P–O–P bridge and those of external PO_3 groups and the influence of Ca on the vibrational frequencies of the anion. Within this approximation, the stretching frequencies observed by IR and Raman spectroscopy depend on the P–O–P angle θ and the force constant k of the P–O bond.

Lazarev suggested an empirical relationship between the P–O–P angle θ and a quantity Δ [Equation (2)] that eliminates the contribution of the force constant k.[42]

$$\Delta = (\nu^{as}POP - \nu^{s}POP)/(\nu^{as}POP + \nu^{s}POP) = f(\theta) \quad (2)$$

The Lazarev relationship has been applied to pyrosilicates, pyrogermanates and pyrophosphates and was satisfactorily obeyed by a large majority of compounds, al-

though a few of them exhibited a significant deviation from the main curve.[37] In those cases, the two approximations mentioned above could explain the differences observed. However, the relationship seems to be confirmed and is linear for pyrophosphate compounds with dichromate structure.

The Lazarev relationship was applied to m-CPPD with $100\Delta = 11.54$, and a θ angle of 133.6° was determined from the plot published by Rulmont et al.[37] This value was compared to those of the other calcium pyrophosphate compounds α-$Ca_2P_2O_7$, β-$Ca_2P_2O_7$, m-CPPT β and t-CPPD, which are 130.0, 130.5 and 137.8 (two sites), 134.1 and 123°, respectively. The configuration of the $P_2O_7^{4-}$ anion in m-CPPD was determined to be closer to those of anhydrous or tetrahydrated compounds than to that of the other dihydrate, t-CPPD, or even other types of dihydrates such as $Mn_2P_2O_7{\cdot}2H_2O$, $Fe_2P_2O_7{\cdot}2H_2O$, $Co_2P_2O_7{\cdot}2H_2O$ and $Mg_2P_2O_7{\cdot}2H_2O$ (127.5, 125.9, 126.2 and 125.7°, respectively), all of which exhibited much lower values for the P–O–P angle.[30–32,35]

Differences between pyrophosphate phase structures have already been reported for anhydrous compounds by Brown and Calvo.[43] Crystals of the composition $X_2Y_2O_7$ (Y = Si, P, As, Ge) with an ionic radius for X of less than 0.97 Å (X = Mg, Mn, Fe, Co, Ni, Cu, Zn) are isostructural with thortveitite ($Sc_2Si_2O_7$) with X–O–X bond angles of 140–180°, an O–Y···Y–O torsion angle of 60° (staggered conformation), and the YO_4 tetrahedra shows a very low degree of distortion, However, those in which X has an ionic radius greater than 0.97 Å (X = Ca, Sr, Ba) usually crystallise with a dichromate structure with a Y–O–Y angle of ca. 120–130°, an O–Y···Y–O torsion angle of 0–30° (eclipsed conformation) and distorted YO_4 tetrahedra.[21] Unlike the corresponding anhydrous compounds, $Mn_2P_2O_7{\cdot}2H_2O$, $Fe_2P_2O_7{\cdot}2H_2O$, $Co_2P_2O_7{\cdot}2H_2O$ and $Mg_2P_2O_7{\cdot}2H_2O$ present a dichromate structure with O–P···P–O torsion angles and P–O–P angles between those of t-CPPD and α-$Ca_2P_2O_7$.

Moreover, Mandel correlated this value of the θ angle to a deformed tetrahedra and a P–O distance in the bridge between 1.61 and 1.63 Å.[28] According to Cruickshank, this relationship is based on the dπ–pπ overlap in the P–O bonds.[44] A P–O–P angle of ca. 130° would degrade dπ–pπ overlap in the P–O bonds in the bridge and, therefore, result in a larger P–O distance.

For an angle of ca. 180°, the P–O bonds receive some π character from the p orbital in the P–O–P plane as well as from the p orbital perpendicular to the plane, and the bond length then decreases. At the P–O–P angle limit of 180°, both p orbitals on the oxygen atom perpendicular to the P–O–P line would share fully in the two π systems. This case corresponds to the thortveitite $Sc_2Si_2O_7$ structure, in which the PO_4 tetrahedra show a very low degree of distortion, as in the β-$Mg_2P_2O_7$ structure.

For an angle of ca. 130°, the π character decreases and the bond length is supposed to increase.[45]

A comparison of the Raman and IR bands of the PO_3 deformation modes between 700 and 400 cm^{-1} and the stretching modes between 1250 and 950 cm^{-1} could also be used to determine if the pyrophosphate compounds have a centrosymmetric structure. The coincidence of the Raman and IR bands in this domain confirms that the structure is not a centrosymmetric thortveitite structure.

Chemical analyses were performed to determine the composition of the as-synthesised CPP phases. We first considered that the conditions of synthesis used in these preparations of calcium pyrophosphate phases could lead to hydrolysis of pyrophosphate anions into two hydrogen phosphate anions [Equation (3)].

$$P_2O_7^{4-} + H_2O \rightleftharpoons 2HPO_4^{2-} \quad (3)$$

This hydrolysis reaction has been reported to occur through two different processes: as an intracrystalline process referred to as internal hydrolysis and a process in solution referred to as external hydrolysis.[24]

Internal hydrolysis of pyrophosphate was observed in amorphous calcium pyrophosphate at a moderate temperature of 37 °C. Water molecules contained in the bulk solid react with nearby pyrophosphate molecules to form small amounts of phosphate anions.[24] However, the phenomenon is negligible under 140 °C.

At lower temperatures, a homogeneous hydrolysis of $P_2O_7^{4-}$ ions in solution occurs and is favoured by acidic pH. These reaction conditions were implemented for the chemical analysis of $P_2O_7^{4-}$ ions in the as-synthesised CPP samples (see Experimental Section). Significant amounts of orthophosphate anions could be produced by this process during the synthesis depending on the pH and temperature used.[46]

Phosphorus titrations, of orthophosphate (PO_4^{3-} and HPO_4^{2-}) and pyrophosphate ($P_2O_7^{4-}$) ions, were performed to assess the percentage of pyrophosphate hydrolysed during the synthesis (Table 4). The results indicate that pyrophosphate hydrolysis is very limited: ca. 2% of the $P_2O_7^{4-}$ ions of each crystalline CPP phase synthesised were titrated as hydrolysed. This hydrolysis could have occurred during the preparation of the sample for titration or during the synthesis. In any case, the quantity of orthophosphate ions detected corresponds to the detection limit of the method.

Table 4. Phosphorus (as $P_2O_7^{4-}$, PO_4^{3-} or HPO_4^{2-} ions) and calcium contents in the four synthesised hydrated CPP phases determined by chemical analyses.

	P as $P_2O_7^{4-}$ [wt.-%]	P as PO_4^{3-} or HPO_4^{2-} [wt.-%]	Ca as Ca^{2+} [wt.-%]	Ca/P
t-CPPD	21.2	0.29	27.6	1.01
m-CPPD	21.2	0.57	27.6	1.01
m-CPPT β	19.1	0.23	24.6	1.00
a-CPP	19.5	0.86	25.2	1.00

The present synthesis conditions of temperature and pH do not allow significant hydrolysis of pyrophosphate anions, even under the more extreme conditions (acidic pH and high temperature). The significantly higher concentration of orthophosphate ions in the a-CPP sample, synthesised at pH 5.8 and 25 °C, indicated either a propensity of the noncrystalline structure to incorporate phosphate ions

or an easier hydrolysis of pyrophosphate ions in this compound after its formation.

The calcium to phosphorus ratio is commonly used to partially identify phases for calcium phosphate compounds and quantify calcium deficiency. Calcium titrations were performed and the results exhibited a characteristic Ca/P ratio of 1 for all calcium pyrophosphate compounds synthesised (Table 4). This indicates that compounds show no calcium deficiency, which could have happened, for example, if protonated pyrophosphate species were present in the precipitates. Moreover, the titration of the crystalline compounds was consistent with the expected water content in the crystalline phases: two H_2O molecules for m-CPPD and t-CPPD and four H_2O molecules for m-CPPT β.

Thermogravimetric analyses were performed to study the evolution of the calcium pyrophosphate hydrates up to 500 °C (Figure 5). The weight loss in the crystalline phases occurred in three steps for the dihydrates and four steps for m-CPPT β.

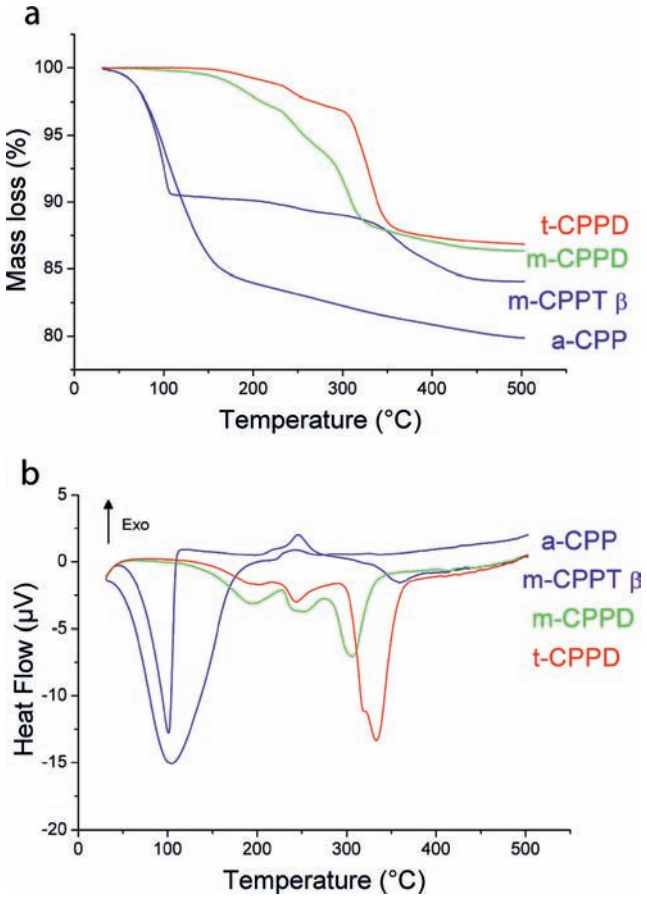

Figure 5. (a) TGA and (b) DTA curves of the pure hydrated calcium pyrophosphate phases synthesised.

Weight losses corresponding to approximately half a H_2O molecule (0.45 H_2O) and one H_2O molecule (1.11 H_2O) were observed for t-CPPD and m-CPPD, respectively, between 30 and 275 °C. Two steps were noted in this range, and they were correlated to wide endothermic peaks on the differential thermal analysis diagram for both compounds. A third step occurred in the range 300–400 °C for t-CPPD and 275–350 °C for m-CPPD, and this led to a dehydrated phase β-$Ca_2P_2O_7$. DTA diagrams indicated that these losses corresponded to two endothermic peaks at 315 and 330 °C for t-CPPD and 300 and 305 °C for m-CPPD.

The thermogravimetric analysis of m-CPPT β has been described previously, and there is an initial weight loss of one H_2O molecule (0.90 H_2O) at ca. 30 °C owing to the instability of the structural water in the m-CPPT β phase.[22,27] This loss at low temperature was detected during the preliminary plateau of the thermogravimetric analysis at ca. 30 °C. The weight loss between 80 and 110 °C corresponds to two H_2O molecules, whereas the one between 300 and 450 °C corresponds to one H_2O molecule and leads to the anhydrous β-$Ca_2P_2O_7$. However, the different mechanisms were not described in the previous studies.

These dehydration processes are in good agreement with the structure of the m-CPPT β phase, which has three different coordinations of H_2O molecules. The slight slope between 110 and 300 °C was decomposed by DTA into two exothermic peaks, which were elucidated by FTIR analysis as an internal hydrolysis described by Equation (3) and the formation of anhydrous dicalcium phosphate or monetite [Equation (4)], identified by XRD and FTIR spectroscopy.

$$Ca_2P_2O_7{\cdot}H_2O \rightarrow 2CaHPO_4 \quad (4)$$

This reaction was followed by a final loss of a water molecule and reconstitution of the $P_2O_7^{4-}$ anions to form to the anhydrous phase β-$Ca_2P_2O_7$ [Equation (5)].

$$2CaHPO_4 \rightarrow H_2O + Ca_2P_2O_7 \quad (5)$$

The reverse reaction occurred at ca. 400 °C and led to the anhydrous phase β-$Ca_2P_2O_7$. This mechanism of dehydration was observed only with the m-CPPT β phase.

The amorphous phase exhibited a continuous weight loss from 30 to 500 °C with a total loss of 3.87 H_2O molecules. This hydration is consistent with the values in the range 3.8–4.2 reported by Slater et al., which varied slightly from sample to sample.[24]

Exothermic peaks appeared between 110 and 250 °C for the DTA of the amorphous phase, in the same way as m-CPPT β and at the same temperature at which m-CPPD and t-CPPD experienced their first step of dehydration. According to the phenomenon observed with the m-CPPT β phase, the exothermic peak could correspond to a partial internal hydrolysis at ca. 220 °C, as reported by Slater et al.[24]

The total weight losses are reported in Table 5 and correspond to the hydration expected for the crystalline phases.

Figure 6 shows the different crystal or particle morphologies of each pure CPP phase as observed by SEM. The crystals of the dihydrated phases were acicular with a large heterogeneity in size. The t-CPPD crystals seemed larger than the m-CPPD crystals, in agreement with former observations.[12,13]

The measured sizes were within the range 1–30 μm for t-CPPD with a maximum width of 5 μm and 1–25 μm for m-

Table 5. Total weight loss in the pure hydrated CPP phases synthesised.

	t-CPPD	m-CPPD	m-CPPT β[a]	a-CPP[a]
H_2O per unit	2.12	2.14	3.73	3.87

[a] Including loss of water during the preliminary plateau at 30 °C: a-CPP 0.31 H_2O and m-CPPT β 0.90 H_2O.

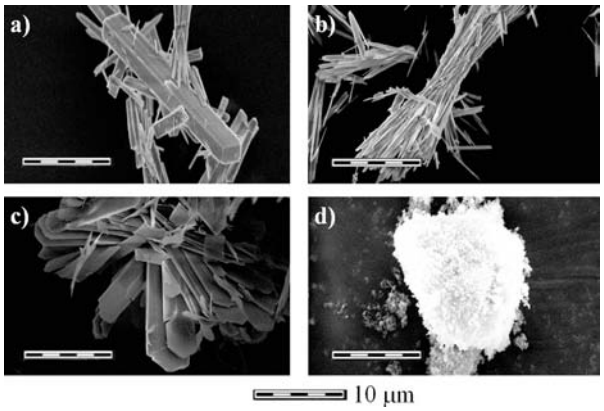

Figure 6. SEM micrographs of the four synthesised hydrated calcium pyrophosphate phases. (a) t-CPPD, (b) m-CPPD, (c) m-CPPT β and (d) a-CPP.

CPPD with a maximum width of 1 μm. The bundle morphologies, which correspond to category two spherulites, are supposed to be caused by growth from a nucleus, possibly a single acicular crystal formed during the first period of the synthesis.[47]

m-CPPT β has a faceted plate morphology with a diameter of up to 20 μm. Balić-Žunić et al.[22] suggested that this morphology was related to the layered structure of this compound.

At higher pH, the m-CPPT β crystals formed had a diameter of ca. 5 μm with irregular shape, and the t-CPPD crystals showed an acicular shape, similar to that of m-CPPD, with fine needles of around 20 μm length. The a-CPP sample contained round particles with diameters of ca. 100 nm.

It has been reported that CPP crystals can have a wide range of sizes and could potentially present different morphologies. Christoffersen et al.[17,18,48] have studied the crystal growth and dissolution of t-CPPD and it presents two different morphologies with different dissolution kinetics. This variety of morphologies could partially explain the different inflammatory potentials between the phases and between samples of a phase.

The specific surface area (SSA) of the four hydrated CPP phases synthesised by the method we set up were determined as $1.3\,m^2g^{-1}$ for t-CPPD, $5.0\,m^2g^{-1}$ for m-CPPD, $4.8\,m^2g^{-1}$ for m-CPPT β and $25.7\,m^2g^{-1}$ for a-CPP. The SSA values are low for the three crystalline phases, as expected, considering their crystal morphology and size (Figure 6). These values are consistent with data already published.[5,14]

In addition to phase structure and morphology, surface area has been suggested as an important factor in the proposed mechanism of inflammation based on the rupture of lysosome phospholipid membranes by pyrophosphate species on the surface of the crystals.[3–5]

Conclusions

The protocol we established allows a fast one-step synthesis of four phases of CPP of biological interest by monitoring the pH and temperature during the synthesis. t-CPPD and m-CPPD, the two phases detected in the joints of arthritic patients, and m-CPPT β and a-CPP, in vitro precursors of the dihydrates, were obtained without intermediates.

The in vitro study of the formation of synthetic and well-characterised hydrated calcium pyrophosphate phases available in large amounts could allow a better understanding of the presence of these phases in vivo in joints and contribute to the clarification of the mechanism by which CPP crystals form in vitro and in vivo. Moreover, fine characterisation of the different synthetic CPP phases could improve their detection in patients suffering from calcium salt crystal diseases.

Experimental Section

General: The hydrated calcium pyrophosphates were synthesised by double decomposition of a potassium pyrophosphate solution and a calcium nitrate solution mixed into a buffer solution at a controlled temperature.

Materials: Anhydrous tetrapotassium pyrophosphate ($K_4P_2O_7$) was prepared by heating dipotassium phosphate (K_2HPO_4, VWR, Analytical reagent, 100 g) at 400 °C for 3 h in a muffle furnace.

Anhydrous tetrapotassium pyrophosphate was analysed by XRD and FTIR spectroscopy. No detectable amount of dipotassium phosphate was observed, and the FTIR spectrum showed the characteristic vibrational modes of $P_2O_7^{4-}$ ions (data not presented).

Calcium nitrate tetrahydrate salt [$Ca(NO_3)_2{\cdot}4H_2O$, Carlo Erba, ACS], ammonia solution (NH_4OH, VWR, 30%) and acetic acid ($C_2H_4O_2$, VWR, NormaPur) were used as received without further purification.

The reagents were stored in a dry place without evidence of degradation after 6 months.

All solutions were prepared with deionised water.

Syntheses: A buffer solution was prepared by adding acetic acid (12 mL) and a variable amount of ammonia solution to water (400 mL). The pH was chosen in a range from 3.6 to 5.8. The solution was stirred and heated to a chosen temperature in the range 25–90 °C (±2 °C).

Calcium and pyrophosphate reagent solutions were prepared separately by dissolving $Ca(NO_3)_2{\cdot}4H_2O$ (7.16 g, 3.03×10^{-2} mol) and $K_4P_2O_7$ (5.00 g, 1.51×10^{-2} mol) in deionised water (200 mL). The reagent solutions were then added simultaneously into the buffer solution by using a peristaltic pump at a constant volumetric flow rate ($4.5\,mL\,min^{-1}$) to maintain the stoichiometry of the system.

The first white precipitate was observed from 3 to 10 min after the beginning of the addition of the reagent solution, depending on the synthesis conditions. The complete addition of the reagent solu-

tions lasted 45 min. After the addition of the reagent solutions was completed, the precipitate formed was left in the mother solution for 10 min at the precipitation temperature.

Filtration was performed by using a Büchner funnel. The precipitate was then washed three times with deionised water and finally dried in an oven at 37 °C overnight. The powder samples were kept at room temperature in sealed vials. No evidence of phase alteration was observed after more than 1 year of storage under these conditions. The yield for this synthesis method was above 90% for the crystalline phases (m-CPPD 4.08 g, t-CPPD 4.13 g, m-CPPT β 4.61 g) and above 85% for a-CPP (4.21 g).

The influence of the concentration of the reagents was studied by varying the amount of potassium pyrophosphate in the reagent solution from 2.5 to 10.0 g in water (200 mL, 37.5 to 150.0 mM, respectively).

Characterisation of Products: Powder X-ray diffraction (XRD) measurements were performed with a Seifert XRD-3000 TT diffractometer with Cu-K_α radiation (Cu-$K_{\alpha1}$ λ = 1.54060 Å and Cu-$K_{\alpha2}$ λ = 1.54443 Å) and equipped with a graphite monochromator. The XRD patterns were obtained in the 2θ range 2–70° with a step size of 0.02° and a scan step time of 16 s at 298 K.

The crystallographic lattice constants were determined by the Jana2006 software (01/07/2011 version).[49] A pseudo-Voigt shape function was assumed and the background was determined manually. The refinement of the parameters was performed in the order scale factor, zero shift, cell parameters, profile parameter and asymmetry parameter. The total number of variables refined was nine.

The FTIR experiments were performed with a Thermo Nicolet 5700 FTIR spectrometer. The spectra were recorded in the 4000–400 cm^{-1} wavelength range with a 64 scan accumulation and 4 cm^{-1} resolution with powder samples in KBr pellets (2 mg of sample in 300 mg of KBr). The peak positions were determined by using second derivation achieved by the Savitzky–Golay routine with a nine-point third-order polynomial smoothing.[50]

Raman microspectroscopy analysis was performed with a Horiba Jobin Yvon Labram HR800 confocal microspectrometer equipped with an AR-diode laser (λ = 532 nm) over a wavenumber range of 55–1750 cm^{-1}.

Thermogravimetric analyses (TGA-DTA) were performed with a Setaram Instrumentation Setsys evolution system from 30 to 500 °C at a heating rate of 5 °C per minute.

Scanning electron microscopy (SEM) observations were performed with a Leo 435 VP microscope. The accelerating voltage was fixed at 7 kV. Samples were silver plated before observation.

A standard spectrophotometric determination of the yellow phosphovanadomolybdic acid complex was used to determine phosphate concentration. Absorption measurements were performed with a Hitachi U-1100 spectrometer set at 460 nm. The pyrophosphate concentrations were determined after hydrolysis of the pyrophosphate ions into phosphate ions. The samples were hydrolysed at 100 °C in acidic medium for 1 hour, and then the phosphate ions were titrated as described above.

The calcium concentrations were determined by complexometry with ethylenediaminetetraacetic acid (EDTA).[51] The calcium and phosphate titrations had estimated standard deviations equivalent to 1% of the reading.

The specific surface areas of the samples were evaluated with a Quantachrome Instruments Monosorb Nova 1000 by using the Brunauer–Emmett–Teller method (nitrogen adsorption) with an estimated standard deviation of 0.5 $m^2 g^{-1}$.

Acknowledgments

The authors thank the Institut National Polytechnique de Toulouse (PRECIPYCA project - BQR INPT 2011), the Centre National de la Recherche Scientifique (CNRS) (CalArthros project – "Longévité et Vieillissement 2010" CNRS interdisciplinary program) and the Agence Nationale de la Recherche (ANR) (CAPYROSIS project – ANR-12-BS08-0022-01) for supporting this research work.

[1] H.-K. Ea, C. Nguyen, D. Bazin, A. Bianchi, J. Guicheux, P. Reboul, M. Daudon, F. Lioté, *Arthritis Rheum.* **2011**, *63*, 10–18.
[2] A. C. Jones, A. J. Chuck, E. A. Arie, D. J. Green, M. Doherty, *Semin. Arthritis Rheum.* **1992**, *22*, 188–202.
[3] L. C. Dijkgraaf, R. S. B. Liem, L. G. M. de Bont, G. Boering, *Osteoarth. Cartil.* **1995**, *3*, 35–45.
[4] N. N. Kohn, R. E. Hughes, D. J. McCarty, J. S. Faires, *Ann. Intern. Med.* **1962**, *56*, 738–745.
[5] M. Roch-Arveiller, R. Legros, B. Chanaud, O. Muntaner, S. Strzalko, A. Thuret, D. A. Willoughby, J. P. Giroud, *Biomed. Pharmacother.* **1990**, *44*, 467–474.
[6] A. Swan, B. Heywood, B. Chapman, H. Seward, P. Dieppe, *Ann. Rheum. Dis.* **1995**, *54*, 825–30.
[7] N. S. Mandel, *Arthritis Rheum.* **1976**, *19*, 439–445.
[8] A. Wierzbicki, P. Dalal, J. D. Madura, H. S. Cheung, *J. Phys. Chem. B* **2003**, *107*, 12346–12351.
[9] F. Martinon, V. Pétrilli, A. Mayor, A. Tardivel, J. Tschopp, *Nature* **2006**, *440*, 237–241.
[10] B. N. Cronstein, *Pharmacol. Rev.* **2005**, *57*, 163–172.
[11] G. Haskó, B. N. Cronstein, *Trends Immunol.* **2004**, *25*, 33–39.
[12] E. H. Brown, J. R. Lehr, J. P. Smith, A. W. Frazier, *J. Agric. Food Chem.* **1963**, *11*, 214–222.
[13] G. S. Mandel, K. M. Renne, A. M. Kolbach, W. D. Kaplan, J. D. Miller, N. S. Mandel, *J. Cryst. Growth* **1988**, *87*, 453–462.
[14] C. I. Winternitz, J. K. Jackson, H. M. Burt, *Rheumatol. Int.* **1996**, *16*, 101–107.
[15] P.-T. Cheng, K. P. H. Pritzker, M. E. Adams, S. C. Nyburg, S. A. Omar, *J. Rheumatol.* **1980**, *7*, 609–616.
[16] P. R. Hearn, R. G. G. Russell, *Ann. Rheum. Dis.* **1980**, *39*, 222–227.
[17] M. R. Christoffersen, N. Seierby, T. Balić-Žunić, J. Christoffersen, *J. Cryst. Growth* **1999**, *203*, 234–243.
[18] M. R. Christoffersen, T. Balić-Žunić, J. Christoffersen, *Cryst. Growth Des.* **2002**, *2*, 567–571.
[19] Y. Z. Liu, A. P. Jackson, S. D. Cosgrove, *Osteoarth. Cartil.* **2009**, *17*, 1333–1340.
[20] P. J. Groves, R. M. Wilson, P. A. Dieppe, R. P. Shellis, *J. Mater. Sci.: Mater. Med.* **2007**, *18*, 1355–1360.
[21] N. L. Davis, G. S. Mandel, N. S. Mandel, R. E. Dickerson, *J. Crystallographic Spectroscopic. Res.* **1985**, *15*, 513–521.
[22] T. Balić-Žunić, M. R. Christoffersen, J. Christoffersen, *Acta Crystallogr., Sect. B* **2000**, *56*, 953–958.
[23] M. R. Christoffersen, T. Balić-Žunić, S. Pehrson, J. Christoffersen, *J. Cryst. Growth* **2000**, *212*, 500–506.
[24] C. Slater, D. Laurencin, V. Burnell, M. E. Smith, L. M. Grover, J. A. Hriljac, A. J. Wright, *J. Mater. Chem.* **2011**, *21*, 18783–18791.
[25] M. R. Christoffersen, J. Christoffersen, *Cryst. Growth Des.* **2003**, *3*, 79–82.
[26] N. S. Mandel, G. S. Mandel, D. J. Carroll, P. B. Halverson, *Arthritis Rheum.* **1984**, *27*, 789–796.
[27] P. Gras, S. Teychené, C. Rey, C. Charvillat, B. Biscans, S. Sarda, C. Combes, *CrystEngComm* **2013**, *15*, 2294–2300.
[28] N. S. Mandel, *Acta Crystallogr., Sect. B* **1975**, *31*, 1730–1734.
[29] K. O. Kongshaug, H. Fjellva, K. P. Lillerud, *Solid State Sci.* **2000**, *2*, 205–214.
[30] J. Oka, a. Kawahara, *Acta Crystallogr., Sect. B* **1982**, *38*, 3–5.
[31] H. Effenberger, F. Pertlik, *Monatsh. Chem.* **1993**, *124*, 381–389.

[32] H. G. Giesber III, M. B. Korzenski, W. T. Pennington, J. W. Kolis, *Acta Crystallogr., Sect. C* **2000**, *56*, 399–400.
[33] K. Brouzi, A. Ennaciri, M. Harcharras, *Phosphorus Sulfur Silicon Relat. Elem.* **2004**, *179*, 1329–1339.
[34] M. Souhassou, C. Lecomte, R. H. Blessing, *Acta Crystallogr., Sect. B Struct. Sci.* **1992**, *48*, 370–376.
[35] S. Schneider, R. L. Collin, *Inorg. Chem.* **1973**, *12*, 2136–2139.
[36] F. Capitelli, M. Harcharras, H. Assaaoudi, A. Ennaciri, A. G. G. Moliterni, V. Bertolasi, *Z. Kristallogr.* **2003**, *218*, 345–350.
[37] A. Rulmont, R. Cahay, M. Liegeois-Duyckaerts, P. Tarte, *Eur. J. Solid State*, *Inorg. Chem.* **1991**, *28*, 207–219.
[38] P.-T. Cheng, K. P. H. Pritzker, *J. Rheumatol.* **1981**, *8*, 772–782.
[39] J. R. Van Wazer, C. F. Callis, *Chem. Rev.* **1958**, *58*, 1011–1046.
[40] B. C. Cornilsen, *J. Mol. Struct.* **1984**, *117*, 1–9.
[41] V. A. Sinyaev, R. Z. Le Geros, L. V. Levchenko, E. S. Shustikova, R. A. Karzhaubaeva, *Russ. J. Gen. Chem.* **2008**, *78*, 864–867.
[42] A. N. Lazarev, *Vibrational Spectra and Structure of Silicates* (English Translation), Consultants Bureau, New York, **1972**.
[43] I. D. Brown, C. Calvo, *J. Solid State Chem.* **1970**, *1*, 173–179.
[44] D. W. J. Cruickshank, *J. Chem. Soc.* **1961**, 5486–5504.
[45] I. D. Brown, R. D. Shannon, *Acta Crystallogr., Sect. A* **1973**, *29*, 266–282.
[46] R. B. Stockbridge, R. Wolfenden, *J. Biol. Chem.* **2011**, *286*, 18538–18546.
[47] L. Gránásy, T. Pusztai, G. Tegze, J. Warren, J. Douglas, *Phys. Rev. E* **2005**, *72*, 011605.
[48] M. R. Christoffersen, T. Balić-Žunić, S. Pehrson, J. Christoffersen, *Cryst. Growth Des.* **2001**, *1*, 463–466.
[49] V. Petricek, M. Dusek, L. Palatinus, *Jana2006*, *The Crystallographic Computing System*, Institute of Physics, Praha, **2006**.
[50] A. Savitzky, M. J. E. Golay, *Anal. Chem.* **1964**, *36*, 1627–1639.
[51] G. Charlot, *Chimie Analytique Quantitative*, Masson, Paris, **1974**.